A nodal loop crystal with minimal symmetry: triclinic CaAs$_3$

Y. Quan and Z. P. Yin
Department of Physics and Center for Advanced Quantum Studies,
Beijing Normal University, Beijing 100875, China

W. E. Pickett
Department of Physics, University of California Davis, Davis CA 95616
(Dated: August 31, 2016)

The electronic spectra of topological insulators and semimetals are intimately connected with crystal symmetry, suggesting the question: what is the minimum symmetry required for topological character, and can one find an example? Triclinic CaAs$_3$, in space group $P\bar{1}$ with only a center of inversion, has been found to display, without need for tuning, a nodal loop of accidental degeneracies with topological character, centered on one face of the Brillouin zone throughout which is otherwise fully gapped. The small loop of degeneracies is very flat in energy, yet is cut four times by the Fermi energy, a condition that results in an intricate repeated touching of inversion related pairs of Fermi surfaces. Spin-orbit coupling lifts the accidental degeneracies, leaving a topological insulator phase. CaAs$_3$ is shown to be the lowest symmetry topological material possible, and is a unique case of a nodal loop semimetal converted to topological insulator by spin-orbit coupling.

PACS numbers:

Dirac, Weyl, and nodal loop semimetals with topological character[1] are complementing the great interest in topological insulators, both because of their novelty and that they display Fermi arcs or points at boundaries that provide new surface properties. The crystal symmetries that enable, or in common parlance protect, the necessary degeneracies is a crucial aspect of their occurrence and their theoretical description.

When the little group at wavevector $\vec{k}$ contains only the identity, the Hamiltonian H has matrix elements between states with neighboring eigenvalues and anticrossings occur as some parameter of H is varied. von Neumann and Wigner first investigated the conditions under which degeneracies nevertheless occur, so-called accidental degeneracies,[2] where matrix elements vanish for no reason. Herring generalized their arguments to accidental degeneracies in three dimensional (3D) crystals,[3,4] with some extension by Blount.[5] Herring pointed out, for example, that a mirror plane provides a natural platform for a ring of degeneracies. If a band with even mirror symmetry is higher in energy than a band of odd symmetry at $\vec{k}_1$ but lower at $\vec{k}_2$ (both on the mirror plane), then due to the continuity of eigenvalues and differing symmetry, on any path connecting them there must be a point of degeneracy. The locus of such degeneracies maps out either a loop encircling one of the points, or an extended line from zone to zone separating the two points (which, considering periodicity, also becomes a closed loop topologically).

The topologically singular nature of such nodal loops was established by Berry,[6] and Allen demonstrated[7] how these loops of degeneracies are destroyed by spin-orbit coupling (SOC). Burkov *et al.* illustrated that a band touching point would connect generic Fermi surfaces.[8] Such nodal loops should be common, and indeed have been found even in high symmetry elemental metals.[9] Nodal loop semimetals based on crystal symmetries, especially mirror symmetries, have appeared in several models[8,10–14] and crystal structures.[15–25]

An early report before the modern rediscovery[8] of nodal loops was of a pair of coinciding Fermi rings – a nodal ring essentially coinciding with the Fermi energy – discovered in calculations for compensated semimetal SrVO$_3$ quantum confined within insulating SrTiO$_3$,[15] where mirror symmetry was a central feature. What is unlikely but not statistically improbable is: (1) having the loop cut by the Fermi energy while (2) the remainder of the Brillouin zone is gapped. Such loops will have real impact, and possible applications, when they are the sole bands around the Fermi energy (E_F), because they generate topological character with corresponding boundary Fermi arcs or points.
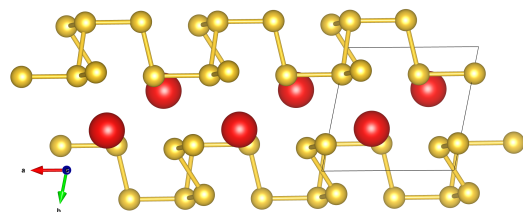

FIG. 1: Crystal structure of CaAs$_3$, viewed in the *b-c* plane. Arsenic atoms (yellow) form two-dimensional chains similar to black phosphorus. The center of inversion lies midway between neighboring Ca ions (shown in red).

Among his several results relating crystal symmetries to accidental degeneracies Herring,[3,4] elaborated somewhat by Blount,[5] considering time reversal ($\mathcal{T}$) invariant systems, found that inversion symmetry $\mathcal{P}$ alone is sufficient to allow nodal loops of degeneracies, a result extended recently.[8,11,12] Simply stated, $\mathcal{P}$ symmetry leads to a real Bloch Hamiltonian $H(\vec{k})$ if the center of inversion is taken as the origin. The minimal 2×2 Hamiltonian then has the form $H(\vec{k}) = f_k\sigma_x + g_k\sigma_z$ (neglecting

spin for the moment) with real functions f_k, g_k; $\vec{\sigma}$ represents the Pauli matrices in band space. Degeneracy of the eigenvalues $\varepsilon_k = \pm(f_k^2 + g_k^2)^{1/2}$ requires $f_k = 0 = g_k$, two conditions on the 3D k-vector, giving implicitly (say) $k_y = \mathcal{K}(k_x, k_z)$ for some function $\mathcal{K}$. This condition either has no solution, or else corresponds to a loop $\mathcal{L}$ of degeneracies. Allen has given a constructive prescription[7] for following the nodal loop once a degeneracy is detected.

Any such loop will not lie at a single energy, and as mentioned only acquires impact when it crosses E_F. This intersection results in a pair (or an even number) of points where, in the absence of spin-orbit coupling (SOC), the valence and conduction band Fermi surfaces touch. The dispersion at the Fermi contact points will, barring accidents of zero probability, be massless in all three directions.[4] At this level the nodal loop semimetal is actually a 3D Weyl semimetal. Also before the rediscovery of nodal loops, Allen described[7] for this same $\mathcal{P}, \mathcal{T}$- invariant case the unusual effect of spin-orbit coupling on the nodal loop and its topological nature, which we return to later.

Topics that have not been addressed are: how little symmetry is necessary for topological character to be retained, what are the consequences, and can an example with minimum symmetry be found? The line of reasoning above applied to the case of no inversion center (*i.e.* no crystal symmetry at all) dictates that all of the coefficients of $\sigma_x, \sigma_y, \sigma_z$ in $H(k)$ vanish. Accidental point degeneracies are thus possible but probably rare, while a line of degeneracies occurs with zero probability.

Discovery and study of topological nodal line semimetals protected by crystal symmetry is developing rapidly.[9,17,22,23,25] The class TPn (T=Nb, Ta; Pn=P, As) lacks an inversion center but contains several crystalline symmetries enabling nodal loops.[18–25] The cubic antiperovskite Cu_3PdN contains nodal loops in a background of metallic bands,[11,17] the $BaTaSe_4$ family has nodal loops in its band structure enabled by symmetry, and as mentioned cubic elemental metals contain loops within their metallic bands.[9] Here we show that triclinic $CaAs_3$ is an example of a minimal symmetry nodal loop crystal that moreover becomes gapped by SOC to become a topological insulator.

$CaAs_3$ and three isovalent tri-arsenides ($Ca \rightarrow Sr$, Ba, Eu) were synthesized more than thirty years ago, with their structure, transport, and optical properties studied only by Bauhofer and collaborators.[29,30] $CaAs_3$ is the sole triclinic member of this family, with space group $P\bar{1}$ (#2) containing only an inversion center, lying midway between Ca sites.[29] This compound is insulating in transport measurements[29] but curiously displays[30] in far infrared reflectivity a Drude weight corresponding to 10^{17}-10^{18} carriers per cm^3.

The sole symmetry condition in $P\bar{1}$ symmetry on the energy bands is $\varepsilon_{-k} = \varepsilon_k$ (by inversion and by time reversal). This "simplicity" indicates that "symmetry lines" are simply convenient lines with no symmetry. $P\bar{1}$ symmetry does however provide eight inversion symmetry invariant momenta (ISIM) $m\frac{a^*}{2} + n\frac{b^*}{2} + p\frac{c^*}{2}, m, n, p =$
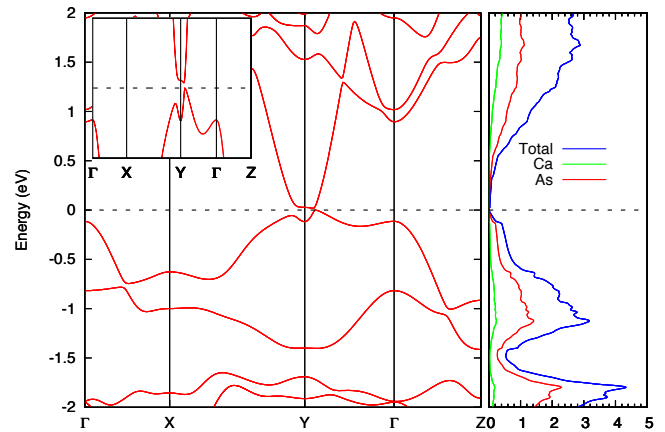

FIG. 2: Band structure of $CaAs_3$ along a few special direction, from a GGA+mBJ+SOC calculation, and (right panel) the density of states. The region of interest lies near the $Y = \vec{b}^*/2$ zone boundary (ISIM) point. Band inversion at Y can be easily imagined by ignoring the mixing that causes anticrossing along the $X - Y$ direction. Even without SOC, a gap of ~ 10 meV separates occupied and unoccupied states along the Y-Γ direction (see inset).

0, 1, in terms of the primitive reciprocal lattice vectors a^*, b^*, c^*. At these ISIMs, which are the analog of (and equivalent to) the time reversal invariant momenta (TRIMs) important in topological insulator theory,[31] eigenstates have even or odd parity. Isolated nodal loops must be centered at an ISIM, otherwise they occur in inversion related pairs. Due to the low symmetry, finding unusual characteristics (viz. the occurrence of and center of a nodal loop) necessitates meticulously searching in band inversion regions.

The linearized augmented plane wave method as implemented in WIEN2k[32] was applied with the generalized gradient approximation (GGA) exchange-correlation potential.[33] $R_m K_{max}$=7 is a sufficient cutoff for the basis function expansion in this sp electron material. Studies have shown that GGA underestimates relative positioning of valence and conduction bands in semiconductors and semimetals, and that the modified Becke-Johnson (mBJ) potential provides a reasonably accurate correction.[36] Thus we rely on the GGA+mBJ combination throughout. Spin-orbit coupling (SOC) is added as indicated and plays a substantial role.

The $CaAs_3$ band structure in a few special directions, and density of states (DOS) in the energy range from -2 eV to 2 eV, shown in Fig. 2, suggests small-gap insulating character. $CaAs_3$ is a Zintl compound, in which the cation is ionized to Ca^{2+} and both valence and conduction bands around the gap are As $4p$ derived. Valence and conduction bands are separate except for an evident band inversion (*before* consideration of SOC) at the $Y \equiv \vec{b}^*/2$ zone boundary ISIM point. Note that with non-ISIM points having a trivial little group, bands do not cross except at accidental degeneracies, and these will occur on a special line with zero probability. The

combination of $\mathcal{P}$ symmetry and periodicity is enough to ensure that band energies at $\vec{b}^*/2 \pm (0, \delta k_y, 0)$ are equal, thus (relative) band extrema occur at the ISIMs, and can be observed at X, Y, Z, and Γ in Fig. 2.
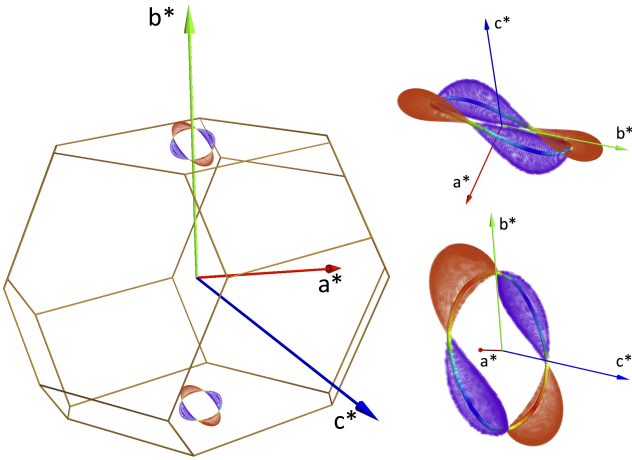

FIG. 3: Left panel: Brillouin zone of CaAs$_3$, showing that the nodal loop is centered at Y on the top (and bottom) face of this view of the zone. Right panels: two perspective views of the nodal line enclosed within the Fermi surfaces, with electron and hole surfaces denoted by different colors.

Searching the band inversion region, a loop $\mathcal{L}$ of accidental degeneracies centered at Y was discovered. Its position in the BZ is shown in Fig. 3 together with two perspective views of the Fermi surfaces (FSs). The loop, resembling a nearly planar lariat, is cut by E_F at not two but *four* points, each point being a touching point for a hole and electron FS (guaranteed by the nodal degeneracies). At this level (no SOC) the spectrum is that of a semimetal with FSs touching at sharp points. The loop energy lies in the -20 meV to +20 meV range, making it a very flat nodal loop in the energy domain as well as in momentum space. Projected onto a surface, $\mathcal{L}$ will be roughly elliptical (or possibly slender figure-eight like).

The surface Fermi arcs of some 3D Weyl semimetals are now well studied. The analogous states in nodal loop semimetals have been discussed by Burkov *et al.*[8] Projected onto a surface, $\mathcal{L}$ will enclose an area within which topologically-required surface states reside. We refer to this partial band covering only a (small) part of the surface zone as a "patch," the states within the patch have sometimes been referred to as drumhead states. A plot along a k-line crossing the patch will reveal a surface band starting at the edge of this patch and ending when the k-line leaves the patch. Considering the constant energy contours (potential Fermi lines) in the patch, they may be closed lines or isolated lines that encounter the boundary of the patch. Thus the topological Fermi lines consist of some combination of closed Fermi lines and open Fermi arcs.

These surface band plots along the special directions, viz. $\bar{Y} - \bar{\Gamma} - \bar{X}$, are shown for all three primary surfaces in the left hand panels of Fig. 4. The "nearly flat bands"[8]

are evident in each case. As mentioned, the Fermi energy cuts the nodal loop, hence it intersects the surface patch band resulting in one or more Fermi lines on each surface. Non-topological surface bands such as from dangling bonds may appear as well.

Effect of spin-orbit coupling. The SOC splitting of the atomic As $4p$ level is ξ_{4p}=270 meV. Since each of the bands that are inverted at Y are primarily As $4p$ character, the SOC-driven band shifts will be some appreciable fraction of this value, so given the 40 meV span in energy of the nodal loop, SOC can be expected to have serious consequences, possibly opening a gap. The background band projections, visible in Fig. 4, are indeed substantially altered by SOC. Within the accuracy of the Wannier interpolation and surface projection, the result is consistent with a bulk gap, as indicated by its observed insulating character.[29]

Fig. 4 reveals that the surface band has evolved under SOC, each surface in its own way. The (010) projection leads to a simple crossing of two bands at Γ, while the other projections have bands extending out of the band inversion region. Allen has described[7] the effect of SOC on the topological character of the nodal loop (where special symmetries are not involved, as in CaAs$_3$). Before SOC, the loop has a Berry phase of $\pm\pi$, that is, an integral of the Berry connection around a circuit enclosing the line of degeneracies will give this phase. Since the interband matrix element of the spin-orbit operator vanishes at most at points in the zone, there is zero probability that such a point will lie on a line, thus SOC completely lifts the orbital degeneracy, leaving only Kramers degeneracy as in a conventional semimetal.

Seemingly the Berry phase would therefore change from its quantized value. However, consideration of applied magnetic fields led Allen to discover that a quantized Berry phase remains.[7] Now, if SOC is large enough and $\mathcal{L}$ is flat enough, as it is in CaAs$_3$, the system is gapped. The above-mentioned phase shows up as a Z_2 topological insulator phase, which we find to have topological indices $\nu_0(\nu_1\nu_2\nu_3)$=1(010).

Topological behavior from an effective Hamiltonian. The simple band structure near E_F of CaAs$_3$, with the highest valence band overlapping the lowest conduction band at Y, was fit to a tight-binding model. Away from Y CaAs$_3$ is gapped, making CaAs$_3$ ideal for observing a topological nodal line. For simplicity one can imagine the crystal deformed by an affine transformation to have orthogonal axes. We consider the following two orbital Hamiltonian which reproduces the essential features of the electronic structure of CaAs$_3$. It includes nearest neighbor hopping between like orbitals $\{t_\alpha, \alpha = 1 - 3\}$, and between unlike orbitals $\{t_\alpha, \alpha = 4 - 6\}$ having differing parity:

$$\tilde{H}(\vec{k}) = f(k_a, k_b, k_c)\sigma_x + g(k_a, k_b, k_c)\sigma_z$$
$$f(k_a, k_b, k_c) = t_4 \sin k_a + t_5 \sin k_b + t_6 \sin k_c$$
$$g(k_a, k_b, k_c) = m - t_1 \cos k_a - t_2 \cos k_b - t_3 \cos k_c.$$

This Hamiltonian describes two particle-hole symmetric bands $\pm|g_k|$ with centers separated by $2m$ and coupled
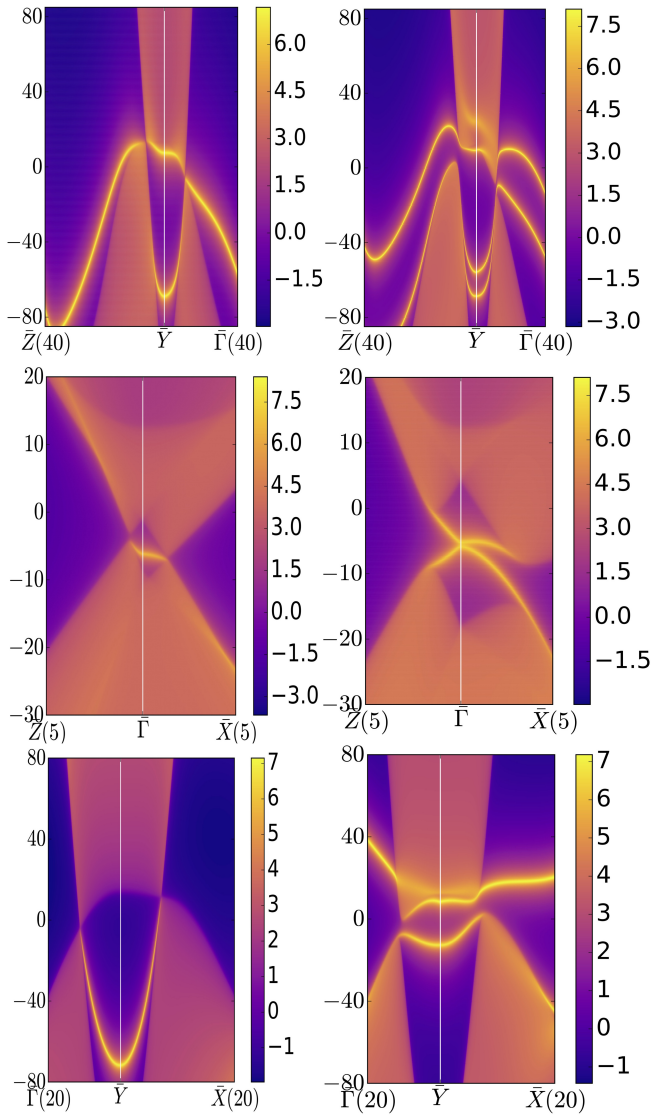
FIG. 4: Edge states (peaks in the spectral density) calculated using the MLWF tight binding representation truncated at the surface. The panels compare spectra before (left) and after (right) inclusion of SOC, for each of the three surface projections. All projections display substantial SOC-induced elaboration of the surface spectrum and near-opening of the bulk gap by SOC. The notation "X(40)" for example, indicates the end point is 40% of the distance toward X.

a closed nodal loop as in $CaAs_3$, or a line extending from zone to zone, which by zone periodicity become closed
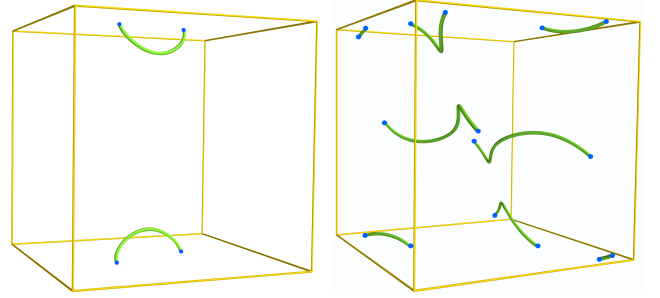

FIG. 5: Nodal lines of accidental degeneracies for the model Hamiltonian. For m=1.44 on the left, a single loop is centered on the ISIM point $\frac{\vec{b}^*}{2}$. The m=0 case is shown on the right, with two pairs of inversion symmetry related lines threading from zone to zone. Due to periodic boundary conditions, the lines in the second case are also topologically closed. As m decreases from 1.44 to 0, the line of degeneracies undergoes a topological transition from an odd number (one) of nodal lines per Brillouin zone finally to an even number (four).

by f_k, with eigenenergies $\varepsilon_{k,\pm} = \pm\sqrt{f_k^2 + g_k^2}$. To mimic $CaAs_3$ we consider the site energy m and hopping parameters (in eV) $m = 1.64$, $t_1 = 0.37$, $t_2 = -0.95$, $t_3 = 0.37$, $t_4 = -0.18$, $t_5 = 0.12$, $t_6 = 0.38$. Degeneracy $f_k = 0 = g_k$ is realized around the nodal loop centered at Y, shown in the left panel of Fig. 5, resembling the nodal loop of $CaAs_3$ pictured in Fig. 3.

The evolution of the loop topology can be followed by varying the band separation $2m$. Two types of lines of accidental degeneracies may emerge from the Hamiltonian:

lines on the 3D-torus, the difference from the former being that they must occur in pairs. In Fig. 5, the two types of loops are plotted in the first Brillouin zone. On the left, where m=1.44, a single loop is centered at Y. Varying m tunes the size of the loop. The right panel in Fig. 5 (m=0) has two pairs of inversion symmetry related nodal loops threading through extended Brillouin zones.

In this work we have studied the electronic and topological properties of $CaAs_3$, which is distinguished by the lowest possible symmetry consisting of only a center of inversion. In the absence of spin-orbit coupling, $CaAs_3$ is a nodal loop semimetal with its loop centered at an inversion symmetry invariant momentum, with its loop of degeneracies crossing the Fermi level four times. Spin-orbit coupling leads not only to destruction of the nodal loop degeneracies but also to a so far unique topological insulating phase. An effective Hamiltonian demonstrates that distinct types of nodal lines will emerge as on-site energies are varied, which provides guidance for engineering topological transitions in $CaAs_3$ by applying external tensile or compressive strains, or by alloying with isovalent atoms on either site.

[1] See, for example, X. Wan, A. M. Turner, A. Vishwanath, and S. Y. Savrasov, Topological semimetal and Fermi-arc surface states in the electronic structure of pyrochlore iridates, Phys. Rev. B **83**, 205101 (2011).

[2] J. von Neumann and E. P. Wigner, On the behavior of eigenvalues in adiabatic processes, Physik. Z. **30**, 467 (1929). Translated in R. S. Knox and A. Gold, *Symmetry in the Solid State* (Benjamin, New York, 1964), p. 167.

[3] W. C. Herring, Accidental Degeneracy in the Energy Bands of Crystals, Phys. Rev. **52**, 365 (1937).

[4] W. C. Herring, On energy coincidences in the theory of Brillouin zones (Lancaster Press, Lancaster, PA, 1937).

[5] E. I. Blount, in *Solid State Physics*, eds. F. Seitz and D. Turnbull (Academic Press, New York, 1962), vol 13, p. 306.

[6] M. V. Berry, Aspects of degeneracy, in *Chaotic Behavior in Quantum Systems*, ed. G. Casatil (Plenum, New York, 1985), pp. 123-140.

[7] P. B. Allen, What happens to geometric phase when spin-orbit interactions lift band degeneracies? arXiv:0709.1457 (2007).

[8] A. A. Burkov, M. D. Hook, and L. Balents, Topological nodal semimetals, Phys. Rev. B **84**, 235126 (2011).

[9] M. Hirayama, R. Okugawa, T. Miyake, and S. Murakami, Topological Dirac nodal lines in fcc calcium, strontium, and ytterbium, arXiv:1602.06501.

[10] M. Phillips and V. Ali, Tunable line node semimetals, Phys. Rev. B **90**, 115111 (2014).

[11] Y. Kim, B. J. Wieder, C. L. Kane, and A. M. Rappe, Dirac line nodes in inversion-symmetric crystals, Phys. Rev. Lett. **115**, 036806 (2015).

[12] C. Fang, Y. Chen, H.-Y. Kee, and L. Fu, Topological nodal line semimetals with and without spin-orbital coupling, Phys. Rev. B **92**, 081201 (2015).

[13] T. T. Heikkilä and G. E. Volovik, Nexus and Dirac lines in topological materials, New J. Phys. **17**, 093019 (2015).

[14] K. Mullen, B. Uchoa, and D. T. Glatzhofer, Line of Dirac Nodes in Hyperhoneycomb Lattices, Phys. Rev. Lett. **115**, 026403 (2015).

[15] V. Pardo and W. E. Pickett, Electron Confinement, Orbital Ordering, and Orbital Moments in $d^0 - d^1$ Oxide Heterostructures, Phys. Rev. B **81**, 245117 (2010)

[16] C. Fang, M. J. Gilbert, X. Dai, and B. A. Bernivig, Multi-Weyl topological semimetals stabilized by point group symmetry, Phys. Rev. Lett. **108**, 266802 (2012).

[17] R. Yu, H. Weng, Z. Fang, X. Dai, and X. Hu, Topological Node-Line Semimetal and Dirac Semimetal State in Antiperovskite Cu_3PdN, Phys. Rev. Lett. **115**, 036807 (2015).

[18] S.-M. Huang *et al.*, A Weyl fermion semimetal with surface Fermi arcs in the transition metal monopnictide TaAs class, Nat. Commun. **6**, 1 (2015).

[19] D.-F. Xu, Y.-P. Du, Z. Wang, Y.-P. Li, X.-H. Niu, Q. Yao, P. Dudin, Z.-A. Xu, X.-G. Wan, and D.-L. Feng, Chin. Phys. Lett. **32**, 107101 (2015).

[20] B. Q. Lv *et al.*, Observation of Weyl nodes in TaAs, Nature Physics **11**, 724-727 (2015).

[21] C. Shekhar *et al.*, Extremely large magnetoresistance and ultrahigh mobility in the topological Weyl semimetal candidate NbP, Nat. Phys. **11**, 645 (2015).

[22] H. Weng, C. Fang, Z. Fang, B. A. Berniveg, and X. Dai, Weyl semimetal phase in noncentrosymmetric transition-metal monophosphides, Phys. Rev. X **5**, 011029 (2015).

[23] K.-H. Ahn, K.-W. Lee, and W. E. Pickett, Spin-orbit driven interaction collective electron-hole excitations in a noncentrosymmetric nodal loop Weyl semimetal, Phys. Rev. B **92**, 115149 (2015).

[24] Y. Sun, S.-C. Wu, and B. Yan, Topological surface states and Fermi arcs of the noncentrosymmetric Weyl semimetals TaAs, TaP, NbAs, and NbP, arxiv:1508.06649.

[25] L. X. Yang, Z. K. Liu, Y. Sun, H. Peng, H. F. Yang, T. Zhang, B. Zhou, Y. Zhang, Y. F. Guo, M. Rahn, D. Prabhakaran, Z. Hussain, S.-K. Mo, C. Felser,B. Yan, and Y. L. Chen, Weyl semimetal phase in the non-centrosymmetric compound TaAs, Nat. Phys. **11**, 728 (2015).

[26] M. Neupane *et al.*, Observation of topological nodal fermion semimetal phase in ZrSiS, Phys. Rev. B **93**, 195106 (2016).

[27] H. Huang, J. Liu, D. Vanderbilt, and W. Duan, Topological nodal-line semimetals in alkaline-earth stannides, germanides, and silicides, Phys. Rev. B **93**, 201114 (2016).

[28] J. Zhao, R. Yu, H. Weng, and Z. Fang, Topological node-line semimetal in compressed balck phosphorus, arXiv:1511.05704.

[29] W. Bauhofer, M. Wittmann and H. G. v. Schnering, Structure, electrical and magnetic properties of $CaAs_3$, $SrAs_3$, $BaAs_3$, and EuP_3, J. Phys. Chem. Solids, **42**, 687 (1981)

[30] B. Oleš and H. G. von Schnering, Infrared studies of phonons and free carriers in $CaAs_3$, $SrAs_3$, $BaAs_3$, and α-EuP_3, J. Phys. C **14**, 5559 (1981).

[31] J. C. Y. Teo, L. Fu, and C. L. Kane, Surface states and topological invariants in three-dimensional topological insulators: Application to $Bi_{1x}Sb_x$, Phys. Rev. B **78**, 045426 (2008).

[32] P. Blaha, K. Schwarz, G. Madsen, D. Kvasnicka and J. Luitz, WIEN2k, An Augmented Plane Wave + Local Orbitals Program for Calculating Crystal Properties (Karlheinz Schwarz, Techn. Universität Wien, Austria), 2001. ISBN 3-9501031-1-2

[33] J. P. Perdew, K. Burke and M. Ernzerhof, Generalized Gradient Approximation Made Simple, Phys. Rev. Lett. **77**, 3865 (1996).

[34] M. P. López Sancho, J. M. López Sancho, and J. Rubio, Quick iterative scheme for the calculation of transfer matrices: application to Mo (100), J. Phys. F: Metal Phys. **14**, 1205 (1984).

[35] K. Momma and F. Izumi, J. Appl. Crystallogr. **44**, 1272 (2011).

[36] H. Zhang and S.-C. Zhang, Phys. Status Solidi RR **7** 1862-6270 (2013)

[37] Jianzhou Zhao, Rui Yu, Hongming Weng, Zhong Fang arXiv:1511.05704

[38] H. Weng, Y. Liang, Q. Xu, R. Yu, Z. Fang, X. Dai, and Y. Kawazoe, Topological node-line semimetal in three-dimensional graphene networks, Phys. Rev. B **92**, 045108 (2015).

[39] C. Fang, Y. Chen, H.-Y. Kee, and L. Fu, Phys. Rev. B **92**, 081201(R).